Aerospace Science and Technology 50 (2016) 266–271

Contents lists available at ScienceDirect

Aerospace Science and Technology

www.elsevier.com/locate/aescte

Aerothermal exploration of reaction control jet in supersonic crossflow at high altitude

M.S.R. Chandra Murty, Anand V. Bhandarkar, Debasis Chakraborty *

Directorate of Computational Dynamics, Defence Research and Development Laboratory, P.O. – Kanchanbagh, Hyderabad-58, India

ARTICLE INFO

Article history:
Received 25 March 2015
Received in revised form 7 January 2016
Accepted 10 January 2016
Available online 14 January 2016

Keywords:
Multijet
RANS
Aerothermal

ABSTRACT

Multiple reaction control jets injected normal to free-stream is used to manoeuvre aerospace vehicle at high altitudes. Detailed aerothermal analysis of a high speed aerospace vehicle with multiple lateral jets is carried out in its full trajectory covering wide range of Mach numbers and altitudes. Three dimensional RANS simulations with laminar-turbulent transition models are performed at several instances in the flight trajectory using commercial CFD solver. Numerical simulations captured all complex flow phenomena of free stream & multi-jet interaction at high altitudes and its influence on vehicle airframe temperature. Heat flux data base obtained from CFD analysis is used for transient thermal analysis of flight vehicle. High temperature local hot spots in jet wake regions and detailed thermal analysis of total vehicle provided important inputs to the system design.

1. Introduction

Due to operational reasons, aerospace vehicles need to be manoeuvred at high altitudes and conventional control elements like fins and wings etc. become less effective due to decreased air density/dynamic pressure. Side control jets located at various positions of the vehicle are generally employed [1,2] to control the vehicle at high altitudes by injecting high pressure jets transverse to main stream. The side control jet motors are smaller in thrust levels compared to main rocket motor and employ liquid propulsion system in on/off mode depending on flight requirement. In its passive state, side jet control produces no additional drag as none of its components intrudes in the flow path and it has quick response time. Thus lateral jet altitude control has been a preferred choice for aerospace vehicle control at high altitudes.

Detailed review of transverse jet exhausted into supersonic free stream is presented by Champigny and Lacau [1] which describe the complex structure of the flow field consisting of a bow shock, separation region ahead of the jet, barrel shock and counter rotating vortex pair in the wake of the jet. The flow structure of transverse jet in supersonic cross stream is shown schematically by Ben-Yakar et al. [3] and is reproduced in Fig. 1. The operating altitude, free stream Mach number, pressure ratios of the jet and free stream, diameter and shape of the side jet nozzle etc have significant effect on the jet shape and its penetration into the supersonic free stream. Cassel [2] proposed a combination of CFD, wind tunnel and flight testing to understand the complex flow characteristics of jet interaction problem. Recent advances of CFD have enabled direct solution of Jet Interaction (JI) flow field under many circumstances of application interest. Fric et al. [4] categorised vortical flow structure into various groups through experimental observations as a) horseshoe vortex, b) jet shear layer vortices, c) wake regions and d) counter rotating vortex pair (CVP). Effect of freestream boundary layer thickness and momentum ratio (J) on surface pressure field were experimentally investigated by Hojaji et al. [5]. It was found that increased boundary layer thickness ahead of jet causes lesser surface pressure ahead of jet and therefore can affect heat transfer rates. Guelhan et al. [6] measured surface heat transfer rates due to jets injected in hypersonic cross flow. Review of several experimental works on 'Jets in crossflow' can be found in Ref. [7]. Aswin and Chakraborty [8] numerically studied the side jet interaction for missile type configuration experiments performed by Stahl et al. [9]. RANS predictions show reasonable agreement with measured wall pressures, it was found that pitching moment is linearly varying with jet momentum ration. RANS predictions of Sriram et al. [10] could be able to capture important flow features like CVP etc. however they could not explain the large unsteady vortical structures. Though DES, LES and DNS predictions provide better insight of flow features, these methods are prohibitively expensive for high Reynolds number flows in increasing order. Few cases of DES/LES predictions of similar problems are found in Refs. [11–16].

Studies related to multiple jet interactions with free stream at high altitude are rather limited in open literature. When pitch, roll

* Corresponding author. Tel.: +91 40 24583310.
E-mail address: debasis_cfd@drdl.drdo.in (D. Chakraborty).

http://dx.doi.org/10.1016/j.ast.2016.01.004
1270-9638/

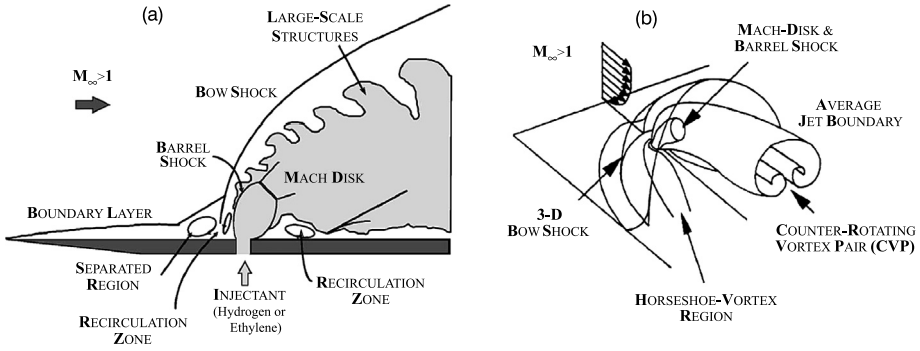

Fig. 1. Schematic of jet injection in high speed cross flow, a) jet structure in axial plane and b) three dimensional features of the jet near field. Figure taken from Ref. [3].

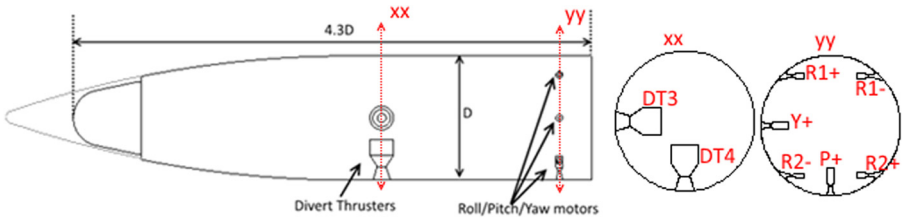

Fig. 2. Schematic of terminal stage of vehicle with Divert and R/P/Y motors.

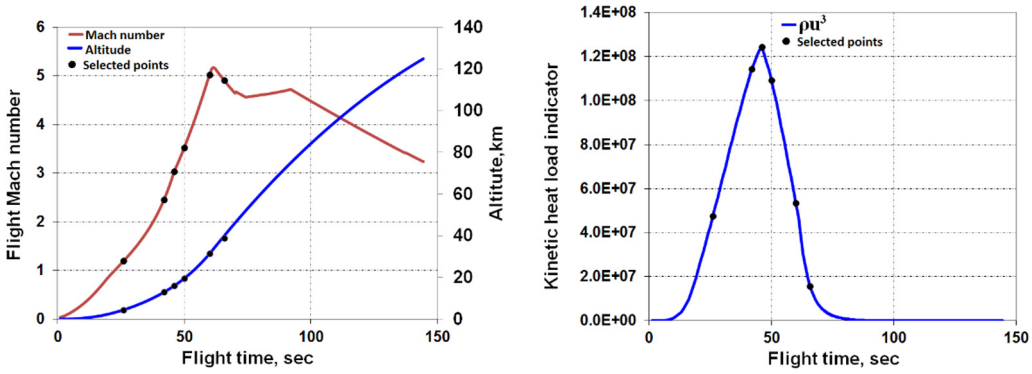

Fig. 3. Flight trajectory and kinetic heat load indicator (ρu^3).

and yaw controls are required simultaneously, a number of hot jets are employed and the motor plumes interact with each other as well as with the free stream. This creates a complex flow pattern around the vehicle body causing some hot gas gazed over the vehicle surface and creates local hotspots which need to be given consideration for thermal safety of the airframe. Saha et al. [17] presented CFD studies giving qualitative features of the multijet–free stream interaction for two discrete altitudes.

In this work, a detailed numerical aerothermal analysis with 3D RANS equations with transition model is presented of an aerospace vehicle in its full trajectory considering different forebody shapes (caused due to heat shield ejection) and multiple lateral jets for simultaneous pitch, roll and yaw control. At select points in the trajectory, steady CFD analysis is carried out and flow field is used for thermal analysis of total vehicle. Flow parameters and skin temperature distributions caused due to aerodynamic heating as well as multijet–freestream interactions are also analysed.

2. The geometry and flight trajectory

The schematic of the vehicle configuration is shown in Fig. 2. After crossing severe aerodynamic heating in the ascent phase, the heat shield (nose cap) is ejected at 39 km altitude leaving the seeker radome exposed to atmosphere and subsequent target locking. A forward facing step is formed at radome and vehicle body joining location. All the reaction control jets are operated after heat shield separation. The divert thrusters are located at CG of the vehicle and Roll/Pitch/Yaw (RPY) thrusters are placed in the rearward portion of the vehicle. After heat shield separation, the vehicle is controlled by reaction control jets i.e., two divert thrusters, four roll thrusters, two pitch and two yaw thrusters. Typical flight trajectory and kinetic heat load indicator (ρu^3) are shown in Fig. 3. Peak Mach number (~5) is achieved at about 25 km altitude.

3. The code and computational details

Reynolds averaged Navier–Stokes equations are solved in a finite volume framework using commercial CFD code 'Ansys Fluent' [18]. Fluid flow equations are solved by employing a cell-centred finite volume method based on the linear reconstruction scheme that allows use of computational elements with arbitrary polyhedral topology, including quadrilateral, hexahedral, triangular, tetrahedral, pyramidal, prismatic and hybrid meshes. Structured computational meshes were generated using ICEMCFD 14.5 [19]. Necessary care is taken in placing the first grid point near the wall boundaries by maintaining proper wall y^+ values and to capture the boundary layer right up to the wall without using any wall functions. Also, very fine grid is provided around jets to resolve high pressure ratios of the jets. Computational domain differs for transonic and supersonic test cases. The inflow boundary, out-

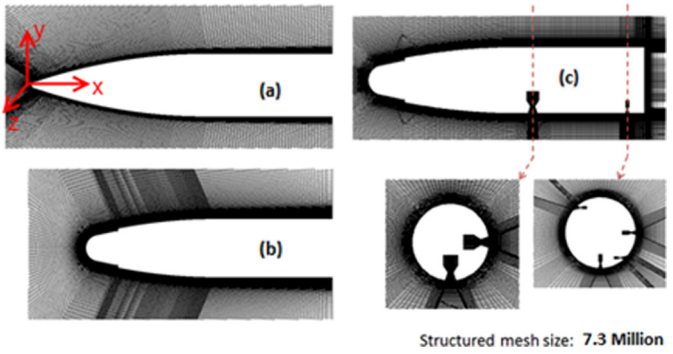

Fig. 4. Computational grid for flow field, a) before nose cap separation, b–c) after nose cap separation.

flow boundary and farfield boundaries are kept at 2D, 1D, 10.5D away from the vehicle surface for transonic cases. The boundaries at kept at 0.25D, 0.5D, 5D distances for supersonic cases without jets and at 2D, 10D, 12D distances for supersonic cases with jets. Maximum grid size of 0.3 Million (585 × 510) is generated for case 1; while 7.3 Million grid is used for case 9 with number of grid points in axial direction about 250. Grid distribution in cross sectional plane varies in axial direction, typically, at DT motor location; the grid size is 250(radial) × 250(circumferential). Computational grid with 7.3 Million hexahedral cells for external flow simulations are shown in Fig. 4 and structured computational grid of size 2.3 Million in solid zones is shown in Fig. 5 that is used for thermal analysis of missile airframe. Different sections in the airframes are made of steel, aluminium, titanium and quartz and are marked in the figure. Two species, namely, free stream air and high temperature nozzle exhaust are considered in the simulation. Density based implicit coupled solver is chosen for solving the governing equations of continuity, momentum and energy simultaneously. Second order accurate Roe Flux Difference Splitting scheme [20] is used for spatial discretization of the inviscid fluxes whereas diffusion terms are discretized by 2nd order central differencing scheme. Temporal terms are discretized through 1st order Euler scheme. The discretized algebraic equations are solved using a point-implicit linear equation solver (ILU factorization scheme on a symmetric block Gauss–Seidel) in conjunction with an algebraic multi-grid (AMG) method to accelerate solution convergence. Laminar to Turbulence transition is predicted using correlation based 4 Equation Menter's transition SST model [21,22].

RANS simulation matrix is shown in Table 1. Nine different trajectory conditions covering different altitudes (4.4–53 km), different free stream Mach number (1.2–4.5) and angles of attacks (0°–7°) are considered. Appropriate vehicle geometry and motor operating conditions are also considered. Following the procedure in Ref. [23], two different simulations (one adiabatic, one isothermal) are carried out at every trajectory point to obtain heat transfer coefficient for thermal analysis. Flow variables are kept fixed at the inflow plane as the inflow conditions are supersonic and zeroth order extrapolations are applied in the outflow boundary. Free stream conditions are imposed on far field boundaries. No slip condition and appropriate adiabatic/isothermal conditions are imposed in the solid wall. In case of simulation with jets, chamber conditions (stagnation pressure and stagnation temperatures) are imposed in a plane located upstream of nozzle throat. The chamber conditions obtained from chemical equilibrium code CEA [24] and are presented in Table 2. The jet pressure ratios (P_e/P_∞) for different side jet motors (Pitch, Yaw, Roll and divert thruster motors) are given in Table 3 at two different altitudes. The ratios range from 8 and 1300 depending on motor chamber pressure and operating altitudes. Four decade fall of residuals in successive iteration and net mass flux and energy flux imbalance below 0.25% on overall domain boundaries were considered as convergence criteria. The computational methodology was validated by Aswin and Chakraborty [8] against the experimental results of side jet interaction for missile type configuration by Stahl et al. [9]. The computed wall pressures for different angles of attack, ratios of free stream,

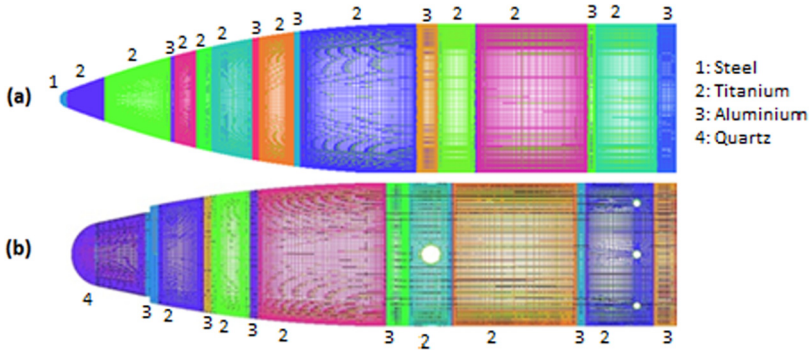

Fig. 5. Computational grid for solid zones, a) before nose cap separation and b) after nose cap separation.

Table 1
RANS simulation matrix, configuration and boundary condition details.

Case no	Time, s	M	Altitude, km	Heat shield	DT motors	R/P/Y motors	AOA, deg
1	26.01	1.19	4.43	yes	OFF	OFF	0
2	42.01	2.46	12.94	yes	OFF	OFF	0
3	46.01	3.03	15.98	yes	OFF	OFF	0
4	50.01	3.53	19.53	yes	OFF	OFF	0
5	60.01	5.03	31.42	yes	OFF	OFF	0
6	65.8	4.90	38.84	yes	OFF	OFF	0
7	65.8	4.90	38.84	no	OFF	OFF	0
8	70	4.65	46.00	no	OFF	ON (P+, Y+, R1+, R2+)	7
9	75	4.56	53.00	no	ON (DT3, DT4)	ON (P+, Y+, R1−, R2−)	7

Table 2
Nozzle inflow conditions.

Parameter	Pitch, Yaw, Roll and Divert thrusters	
Total pressure (bar)	30	
Total temperature (K)	2945	
Temperature dependent specific heat, J/kg K	T, K	Cp
	2934	2136
	2640	2016
	1716	1955
Mol. Wt, kg/kg mole	21.021	
Thermal conductivity W/m K	0.22	
Dynamic viscosity, N s/m^2	4.958×10^{-5}	

Table 3
Pressure ratios of R/P/Y/DT motors at different altitudes.

RCS motors	Pressure ratio (P_e/P_{amb})	
	46 km (Case 8)	53 km (Case 9)
Pitch/yaw motor	178.2	434.56
Roll motor	7.878	19.21
DT-motor	532.14	1297.66

jet pressure, number of jets show a very good match with measured wall pressures.

4. Results and discussions

Typical Mach contours in mid plane of vehicle geometry are shown in Fig. 6, for simultaneous firing of Roll–Yaw–Pitch motors (R–Y–P) (case-8) and also for Divert Thrusters Roll–Yaw–Pitch (DT–R–Y–P) motors (case-9). Fig. 7 shows the Mach contours in cross sectional planes xx (DT jets) and yy (R–Y–P jets) (the cross sectional planes XX and YY are marked in Fig. 2) for cases 8 & 9. Important flow features like bow shock ahead of fore-body, flow separation and reattachment near nose cap forward facing step etc. are well captured. Complex flow field is seen around the vehicle body due to injection of supersonic jets into Mach 4.6 freestream.

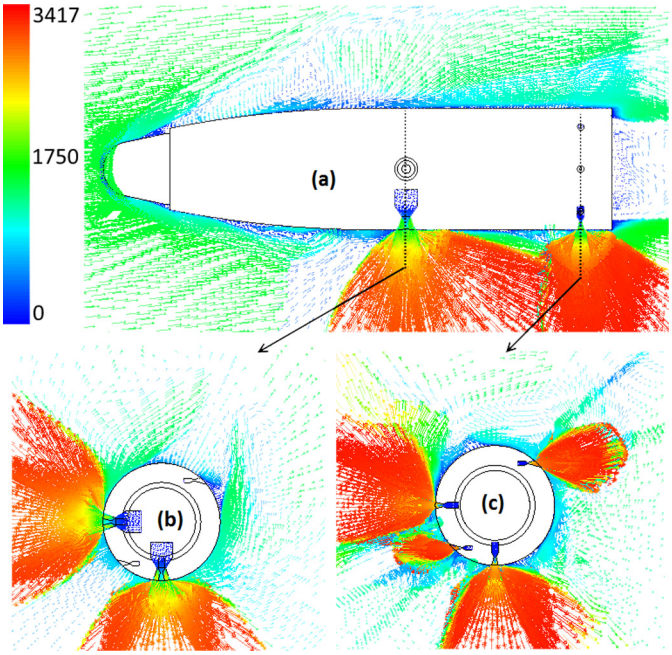

Fig. 8. Velocity vector plot (a) symmetry plane, (b) cross-sectional plane at DT motor location and (c) at P/Y/R motor.

For the case with DT motor jet, the separation point is moved much upstream (Fig. 6(b)) compared to the other case (Fig. 6(a)). The velocity vector plots in the symmetry plane and two cross sectional planes (at DT motor location and P/Y/R thruster location) in Fig. 8 show the separated flow field in the windward and leeward regions. All flow features depicted in Fig. 1 are also captured in the simulation. For 53 km altitude, the point of separation of the flow is 1.3 D and 2 D ahead of DT motor in the windward and leeward direction respectively. The more severe windward separation is due to direct blockage of stronger jet (pressure ratio ∼ 1300);

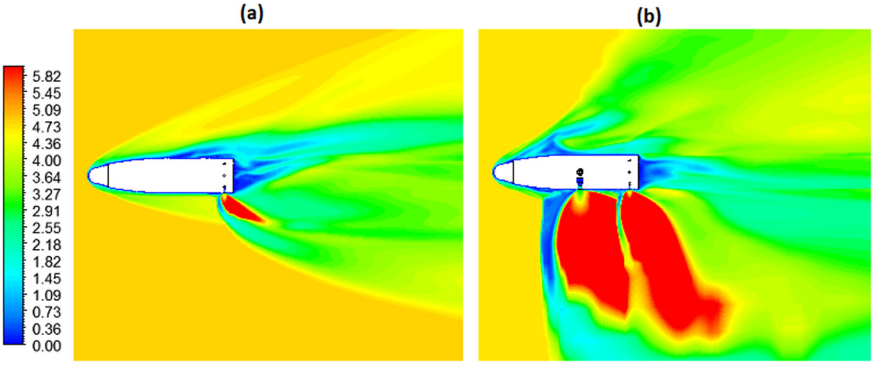

Fig. 6. Mach contours in mid plane a) R–Y–P jets (case-8), b) DT–R–Y–P jets (case-9).

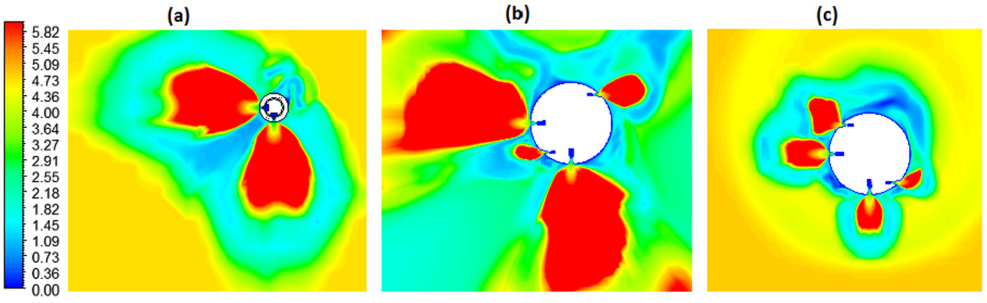

Fig. 7. Mach contours in nozzle cross section planes a) DT jets of C9, b) R–Y–P jets of C9, c) R–Y–P jets of C8.

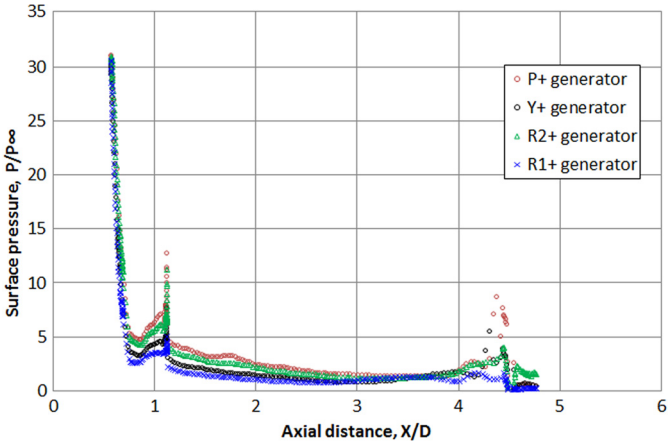

Fig. 9. Vehicle axial surface pressure (P/P_∞) along R–Y–P generators for Case-8.

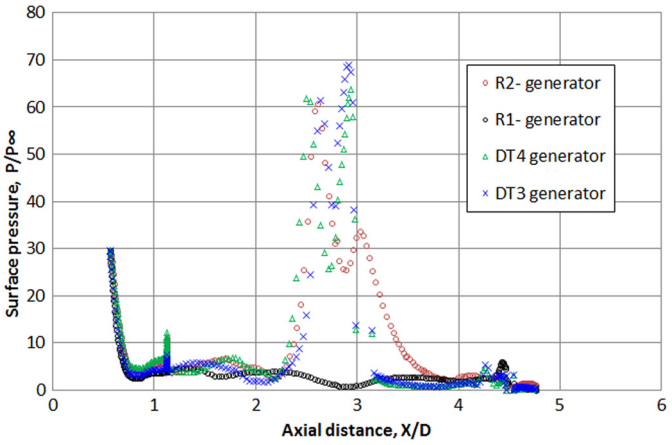

Fig. 10. Vehicle axial surface pressure (P/P_∞) along DT/R generators for Case-9.

whereas the leeward separation is caused due to large disturbance of strong jet injection in the windward side.

Fig. 9 shows the axial surface pressure distribution along four generators passing through R2+, R1+, P+, Y+ motor axis pertaining to case 8. An overall azimuthal symmetry in flow is observed. The jump in pressure at $x/D = 1.2$ is due to the forward facing step appeared due to heat shield ejection. Azimuthal symmetry is lost at 4.5 D where the R–Y–P jets are injected. Fig. 10 shows the axial surface pressure for Case-9 passing through DT and RYP jets. The pressure distribution up to $x/D = 2$ remains similar to the earlier case. But, due to the presence of DT motor jets, large azimuthal variation of surface pressure is observed. The surface pressure along R1-generator is much lower in the region ($x/D = 2.25$–3.75) compared to the other generators. The increase in surface pressure at $x/D = 4.5$ is much smaller compared to $x/D \sim 2$ as the DT motor jets are more powerful than R–Y–P jets. Fig. 11 shows the missile surface temperature as well as the temperature distribution in symmetrical and cross sectional planes. Horseshoe vortex pattern is clearly seen near the DT thruster plume region, while this flow pattern is completely altered near the rear jet region, showing the complexity of the flow.

Multidimensional interpolation of wall heat flux and adiabatic wall temperature history is transferred to material solid zone grid and performed transient 3D thermal analysis. Heat flux is function of 3D space, time, and local wall temperature. Details of the procedure are available in Ref. [25]. Vehicle airframe is made of titanium, aluminium and carbon steel materials. Appropriate temperature dependent thermo-physical properties of materials are employed in analysis. Axial surface temperature profiles with time

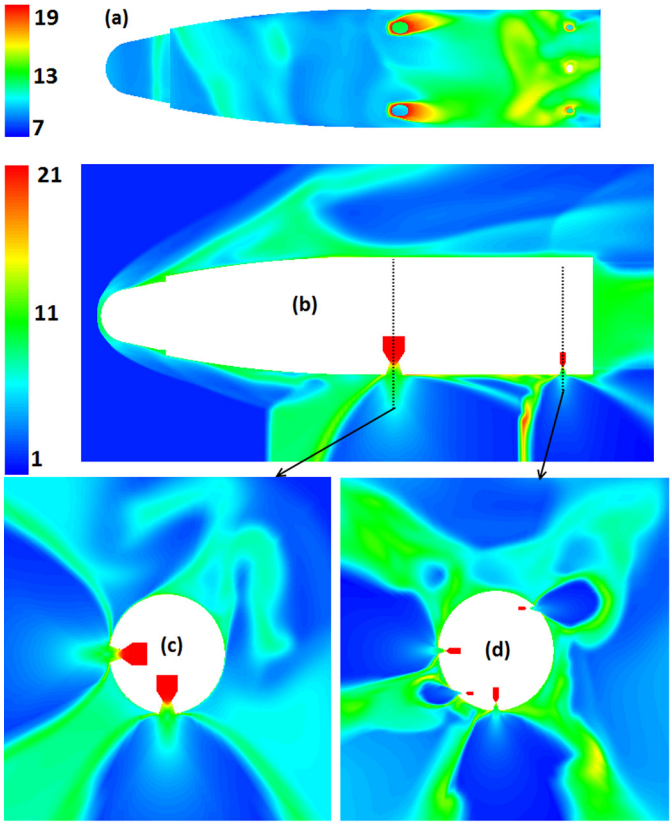

Fig. 11. Wall temperature (T/T_∞) distribution at (a) vehicle surface (b) symmetrical plane (c) cross flow plane at DT motor and (d) cross flow plane at P/Y/R motor.

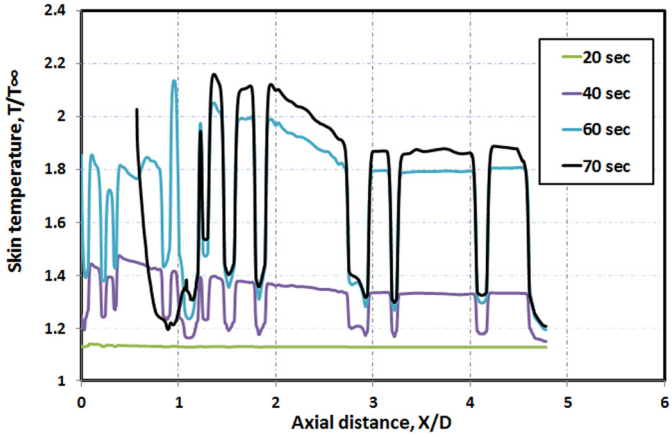

Fig. 12. Vehicle skin temperature (T/T_∞) profiles in axial direction.

are shown in Fig. 12. Due to larger thermal diffusivity of aluminium, temperature dips are seen at section flange joint regions. Maximum skin temperature normalized with free stream static temperature predicted for the aluminium and titanium sections are 1.51 and 2.28 respectively which are below their allowable temperature limits. Surface temperature contours evolution with time is seen in Fig. 13, cold regions are aluminium ribs and hot regions are titanium airframe. Horseshoe vertex pattern is reflected in surface temperature also. Under expanded jets impinge on surrounding vehicle surface that causes sharp rise in material temperature, this phenomenon is clearly seen in surface temperature plot (Fig. 14). These local hot spots are identified from the simulation and special thermal resistant paints were applied during flight experiments.

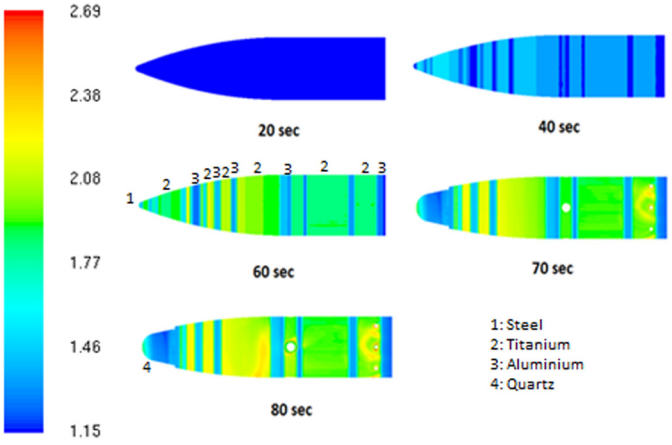

Fig. 13. Vehicle skin temperature (T/T_∞) evolution with time.

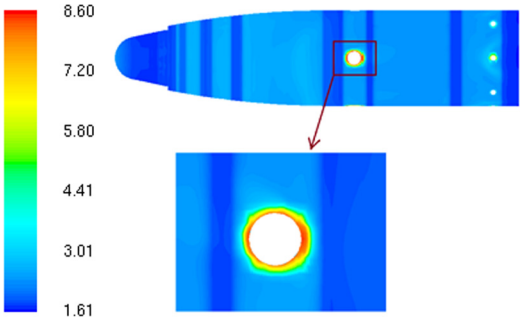

Fig. 14. Local temperature (T/T_∞) hot spots near the reaction control jets.

5. Conclusions

Integrated aerothermal analysis is performed for a high speed aerospace vehicle with multiple lateral jets along its full trajectory from launch to high altitude using high fidelity CFD simulations. Three dimensional RANS equations with laminar-turbulent transition models are solved using commercial CFD solver. Numerical simulations captured all pertinent flow features of multijet–freestream interaction at high altitudes. Horseshoe vortex pattern is found near the DT thruster plume region. For DT motor operation, the windward separation point is moved much upstream compared to the other lateral jets for pitch, roll and yaw control due to direct blockage of stronger DT motor jet (pressure ratio $\sim$ 1300). The DT motor plume broke the azimuthal symmetry of the flow field and also caused severe leeward separation.

CFD generated wall heat flux data along the trajectory and temperature dependent thermophysical properties of the material are used to carryout transient thermal analysis of the vehicle airframe and axial surface temperature profiles with time are determined. Local hot spots caused due to hot plume gazing in the airframe are identified for adequate thermal protection. Present numerical exercise provided insight into complex flow arising due to multiple jets and its impact on vehicle surface temperature.

Conflict of interest statement

This work did not receive any fund from any sources, and there is no conflict of interest with any other work.

References

[1] P. Champigny, R.G. Lacau, Lateral jet control for tactical missiles, Spec. Course Missile Aerodyn. AGARD Rep. 804, 1994, pp. 301–307.
[2] L.A. Cassel, Applying jet interaction technology, J. Spacecr. Rockets 40 (2003) 523–537, http://dx.doi.org/10.2514/2.3992.
[3] A. Ben-Yakar, M.G. Mungal, R.K. Hanson, Time evolution and mixing characteristics of hydrogen and ethylene transverse jets in supersonic crossflows, Phys. Fluids 1994–Present 18 (2006) 026101, http://dx.doi.org/10.1063/1.2139684.
[4] T.F. Fric, A. Roshko, Vortical structure in the wake of a transverse jet, J. Fluid Mech. 279 (1994) 1–47, http://dx.doi.org/10.1017/S0022112094003800.
[5] M. Hojaji, M.R. Soltani, M. Taeibi-Rahni, New visions in experimental investigations of a supersonic under-expanded jet into a high subsonic crossflow, Proc. Inst. Mech. Eng., G J. Aerosp. Eng. 224 (2010) 1069–1080, http://dx.doi.org/10.1243/09544100JAERO748.
[6] A. Guelhan, G. Schuette, B. Stahl, Experimental study on aerothermal heating caused by jet-hypersonic crossflow interaction, J. Spacecr. Rockets 45 (2008) 891–899, http://dx.doi.org/10.2514/1.35899.
[7] E. Hassan, J. Boles, H. Aono, D. Davis, W. Shyy, Supersonic jet and crossflow interaction: computational modeling, Prog. Aerosp. Sci. 57 (2013) 1–24, http://dx.doi.org/10.1016/j.paerosci.2012.06.002.
[8] G. Aswin, D. Chakraborty, Numerical simulation of transverse side jet interaction with supersonic free stream, Aerosp. Sci. Technol. 14 (2010) 295–301, http://dx.doi.org/10.1016/j.ast.2010.02.001.
[9] B. Stahl, H. Esch, A. Gülhan, Experimental investigation of side jet interaction with a supersonic cross flow, Aerosp. Sci. Technol. 12 (2008) 269–275, http://dx.doi.org/10.1016/j.ast.2007.01.009.
[10] A.T. Sriram, J. Mathew, Improved prediction of plane transverse jets in supersonic crossflows, AIAA J. 44 (2006) 405–408, http://dx.doi.org/10.2514/1.17114.
[11] S. Kawai, S.K. Lele, Large-eddy simulation of jet mixing in supersonic crossflows, AIAA J. 48 (2010) 2063–2083, http://dx.doi.org/10.2514/1.J050282.
[12] C. Schaupp, R. Friedrich, Large-eddy simulation of plane jet injection into supersonic turbulent crossflow, in: S. Wagner, M. Steinmetz, A. Bode, M. Brehm (Eds.), High Perform. Comput. Sci. Eng. GarchingMunich 2007, Springer, Berlin, Heidelberg, 2009, pp. 349–363.
[13] C. Kannepalli, S. Arunajatesan, S. Dash, RANS/LES methodology for supersonic transverse jet interactions with approach flow, in: 40th AIAA Aerosp. Sci. Meet. and Exhib. AIAA-2002-1139, American Institute of Aeronautics and Astronautics, n.d.
[14] E.H. Khali, Y. Yao, Mixing flow characteristics for a transverse sonic jet injecting into a supersonic crossflow, in: 53rd AIAA Aerosp. Sci. Meet. AIAA 2015-0545, American Institute of Aeronautics and Astronautics, n.d.
[15] S.-H. Won, I.-S. Jeung, B. Parent, J.-Y. Choi, Numerical investigation of transverse hydrogen jet into supersonic crossflow using detached-eddy simulation, AIAA J. 48 (2010) 1047–1058, http://dx.doi.org/10.2514/1.41165.
[16] S.-H. Won, I.-S. Jeung, J.-Y. Choi, DES investigation of the ignition of hydrogen transverse jet into high enthalpy supersonic crossflow, in: 47th AIAA Aerosp. Sci. Meet. New Horiz. Forum Aerosp. Expo. AIAA-2009-1557, American Institute of Aeronautics and Astronautics, n.d.
[17] S. Saha, P.K. Sinha, D. Chakraborty, Numerical prediction of surface heat flux during multiple jets firing for missile control, J. Inst. Eng. India Ser. C 94 (2013) 85–91, http://dx.doi.org/10.1007/s40032-012-0052-y.
[18] Ansys Fluent 14.5 Theory and Users Guide, Ansys Inc., India, 2013.
[19] ICEM CFD 14.5 Modeling and Meshing Guide, Ansys Inc., India, 2013.
[20] P.L. Roe, Characteristic-based schemes for the Euler equations, Annu. Rev. Fluid Mech. 18 (1986) 337–365, http://dx.doi.org/10.1146/annurev.fl.18.010186.002005.
[21] F.R. Menter, R.B. Langtry, S.R. Likki, Y.B. Suzen, P.G. Huang, S. Völker, A correlation-based transition model using local variables—part I: model formulation, J. Turbomach. 128 (2004) 413–422, http://dx.doi.org/10.1115/1.2184352.
[22] R.B. Langtry, F.R. Menter, Correlation-based transition modeling for unstructured parallelized computational fluid dynamics codes, AIAA J. 47 (2009) 2894–2906, http://dx.doi.org/10.2514/1.42362.
[23] M. ChandraMurty, D. Chakraborty, Thermal response analysis of scramjet combustor walls to high speed turbulent reacting flows, in: Symp. Appl. Aerodyn. Des. Aerosp. Veh., Bangalore, India, 2009.
[24] S. Gordon, B.J. McBride, Computer program for calculation of complex chemical equilibrium compositions and applications, NASA Reference Publication 1311, 1996.
[25] M.S.R. ChandraMurty, Debasis Chakraborty, Thermal response analysis of scramjet combustor walls to high speed turbulent reacting flows, in: Proceedings of SAROD-2009, Bangalore, December 10–12, 2009, pp. 698-710.